

# Neural network space diversity combination and ring coding for multicarrier CDMA over fast fading channels

R.A. Carrasco and R. Uribeetxeberria

**Abstract:** Multicarrier CDMA is a major candidate to fulfil the requirements of 3G mobile systems. A novel scheme is developed combining modulo- $S$  ring TCM with RNN-based adaptive space diversity for multicarrier CDMA systems with single-antenna transmitter and multiple-antenna receiver. The nonlinear RTRL algorithm for antenna diversity combining combats the distortive effects of the communication channel and reduces the interference. Ring TCM channel coding and RNN space diversity are evaluated in 16-QAM multicarrier CDMA systems transmitting over Rician and Rayleigh fast fading channels with a maximum Doppler frequency of 96 Hz. Modulo-4 ring TCM codes of 16 and 64 states have been designed. The RNN system is shown to be superior to the linear algorithms in channels dominated by multipath fading, inter-symbol interference and multiple access interference. The complexity of the RNN structure is comparable to that of the linear techniques. The joint utilisation of RNN based diversity, ring TCM and binary TCM coding schemes has been implemented. Whereas coding and space diversity do not provide sufficient benefit separately, the combination of both produces an increase in performance.

## 1 Introduction

The key features of 3G mobile systems are universal standards for the air interface, global roaming and support of a wide range of data services. Fourth-generation mobile radio systems need to provide high-speed data services to anyone, anytime and anywhere. A multicarrier code division multiple access (CDMA) design can accommodate different data rate users by allocating different numbers of sub-carriers to them depending on their rate needs. Therefore, compatibility with current second-generation systems can be achieved. Multicarrier modulation is also a suitable scheme for high data rates as it enlarges the period of the transmitted data. One of the most attractive features of multicarrier schemes is that the bandwidth of the sub-channel is usually very narrow when compared to the communications channel's coherence bandwidth [1].

Mobile radio communication channels are time-varying, and therefore space diversity combining needs to track the variations of the channels using adaptive signal processing algorithms. This has been traditionally realised using linear filtering structures, whose coefficients are determined in an adaptive manner [2, 3]. The main criteria for optimising the coefficients is based on the minimisation of the mean square error (MSE). The least mean square algorithm has been the most extensively used scheme, owing to its low complexity and robustness [4], despite its slow convergence rate. The more complex recursive least squares filtering [5] provides a much faster rate of convergence. However, minimising the MSE does not guarantee the best error rate performance.

Much better error performance and good convergence can be obtained by using a combined filter structure based on nonlinear processing, in particular using an adaptive artificial recurrent neural network (RNN) [6].

Modulo- $S$  ring trellis coded modulation (TCM) codes are based on algebraic rings of integers modulo- $S$  [7, 8]. Soto and Carrasco have applied genetic algorithm based optimisation techniques to obtain new and efficient modulo-4 ring TCM designs and have searched for the optimum interleaver depth, while keeping the width constant for rectangular multilevel quadrature amplitude modulation (QAM) constellations over fading channels [9, 10]. The interleaver depth was fixed between 40 and 100 due to the nonlinear behaviour of the channel.

In this paper, ring TCM and recurrent neural network (RNN) based space diversity are integrated and modelled in a novel structure with the aim of increasing the channel capacity. The RNN is trained with the real time recurrent learning (RTRL) algorithm [11, 12]. The performance of the proposed systems over Rician and Rayleigh fading cellular mobile communications channels is compared to linear square root Kalman (SRK) [13] combining by means of computer simulations.

## 2 Combined coding and neural space diversity model for multicarrier CDMA

The block diagram of the simulated system is shown in Fig. 1. The transmitter uses ring TCM to encode a  $Z_4$  mapped signal,  $a_i$ , into two 16-QAM symbols,  $x^{(1)}$  and  $x^{(2)}$ . Ring TCM uses three modulo-4 input symbols and obtains four in the output. With four modulo-4 symbols, two points of the constellation can be defined and sent consecutively.

### 2.1 Ring TCM encoding

Fig. 2 shows the general structure of a ring TCM encoder with  $S = 2^{\hat{m}+1}$ . It first maps the binary source into modulo- $S$

© IEE, 2003

IEE Proceedings online no. 20030174

doi:10.1049/ip-com:20030174

Paper first received 14th August 2001 and in revised form 28th June 2002

The authors are with the School of Computing, Staffordshire University, PO Box 334, Beaconside, Stafford ST18 0DG, UK

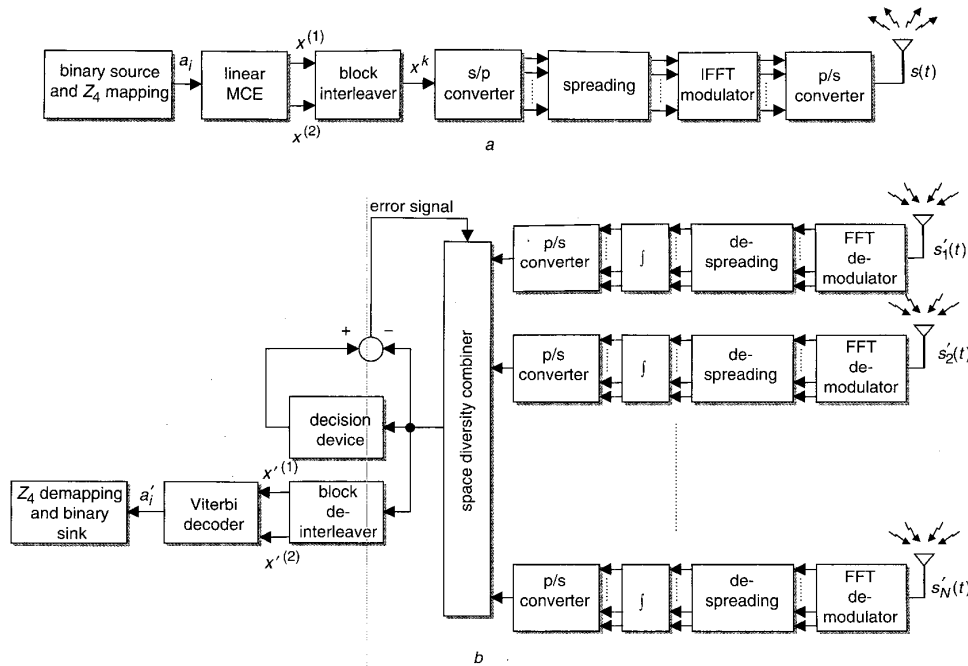


**Fig. 1** Combined coding and space diversity transmitter and receiver for multicarrier CDMA  
 a Transmitter  
 b Receiver

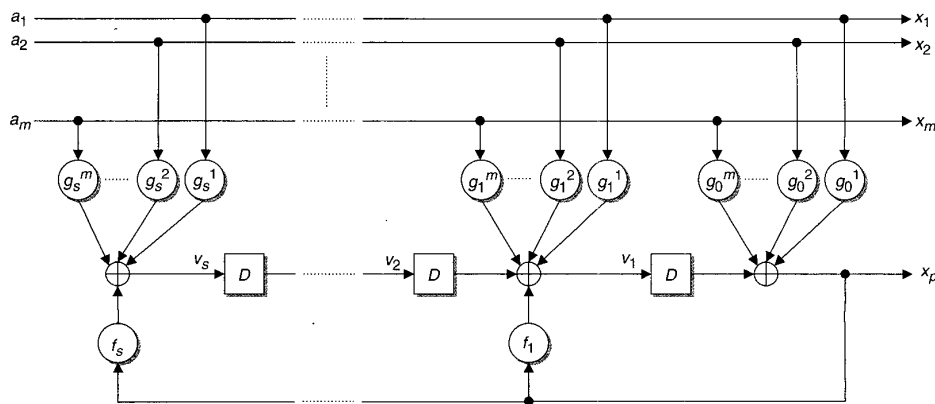


**Fig. 2** Ring-TCM multilevel convolutional encoder

symbols. The multilevel convolutional encoder (MCE) generates  $p \in \mathbb{Z}_S$  encoded output symbols at a time having  $\hat{m} \in \mathbb{Z}_S$  information input symbols. The coefficients of the MCE also belong to  $\mathbb{Z}_S$  and all arithmetic operations performed satisfy the properties of the ring of integers modulo- $S$ . Finally, each one of these coded symbols is associated with a signal of the multilevel QAM signal set and it is sent to the channel. The codes are characterised by the feed-forward and feedback coefficients in accordance with Fig. 2 and the notation  $(g_0^1 g_0^2 \dots g_0^m g_1^1 g_1^2 \dots g_1^m \dots g_s^1 g_s^2 \dots g_s^m / f_1 \dots f_s)$ , where all coefficients belong to  $\mathbb{Z}_4 = 0, 1, 2, 3$  and the arithmetic operations have the properties of the ring of integers modulo-4.

Ring codes suitable for 16-QAM are defined over the ring of integers modulo-4. Ring TCM codes can be considered as  $2(\hat{m} + 1)$ -dimensional TCM codes as  $\hat{m} + 1$

modulo- $S$  coded symbols are transmitted per single trellis branch [9]. To maintain the same average power, a reduction of the Euclidean distance between signals is required in TCM, consequently reducing the noise margin. Multidimensional TCM codes avoid this problem by making use of more dimensions, where doubling the size of the constellation involves a smaller reduction of the Euclidean distance [11].

## 2.2 Multicarrier CDMA

A multicarrier DS-CDMA system has been chosen in this research work and will sometimes be referred to simply as multicarrier CDMA. This scheme was originally proposed for up-link communications channels, because the introduction of OFDM signalling into the DS-CDMA scheme is effective for the establishment of a quasi-

synchronous channel [1, 14]. In this paper, orthogonal Walsh-Hadamard codes are used to spread the low-rate data signal.

The symbols from the MCE are passed to the block interleaver and they are then spread by the Walsh-Hadamard signature sequence. A fast Fourier transformation is recommended for the transmission and reception for high spectral efficiency and not to increase the complexity. The complex transmitted signal for the  $N$ th mobile user can be expressed as follows:

$$s_k(t) = \sqrt{P_s} \sum_{n=0}^{N-1} \left[ a_n^k(t) c_p^k(t) \cos(2\pi f_n t) + j b_n^k(t) c_q^k(t) \sin(2\pi f_n t) \right] \quad (1)$$

where  $P_s$  is the average transmitted signal power,  $b^k(t) = b_p^k(t) + j b_q^k(t)$  is the complex binary data stream for the  $k$ th user,  $c^k(t) = c_p^k(t) + j c_q^k(t)$  is the spreading sequence and  $\omega_n$  represents the angular frequency of modulating carrier  $f_n$ . The in-phase and quadrature components of the user-specific information-bearing signals and their corresponding spreading sequences can be mathematically represented as follows:

$$a_n^k(t) = \sum_{m=-\infty}^{\infty} a_n^k(m) g_T(t - mT) \quad (2)$$

$$b_n^k(t) = \sum_{m=-\infty}^{\infty} b_n^k(m) g_T(t - mT) \quad (3)$$

$$c_p^k(t) = \sum_{m=-\infty}^{\infty} c_p^k(m) p(t - mT_c) \quad (4)$$

$$c_q^k(t) = \sum_{m=-\infty}^{\infty} c_q^k(m) p(t - mT_c) \quad (5)$$

where  $a_n^k(m)$ ,  $b_n^k(m)$ ,  $c_p^k(m)$  and  $c_q^k(m)$  are random variables and  $g_T(t)$  and  $p(t)$  are rectangular pulses of duration  $T$  and  $T_c$ , respectively.  $T_c$  is the chip period and  $T = N\Delta t$ . The best way to deal with transmission impairments is to use independent sequences for the in-phase and quadrature components of the spreading sequences.

The separation between antenna elements has been assumed to be larger than half the wavelength of the transmitted signal to have uncorrelated signals in the antennas. This is desirable to better compensate the fading. The transmitted signals for the  $K_u$  users are passed through statistically independent multipath fading channels. The mobile radio channel corresponding to the  $k$ th user and the  $i$ th antenna can be represented at baseband by the low-pass equivalent complex impulse response

$$h_i^{(k)}(t) = \sum_{l=1}^L A_{il} e^{j\phi_{il}^{(k)}} \delta(t - \tau_{il}^k) \quad (6)$$

where  $L$  is the number of fading paths in the multipath channel, and  $A_{il}$  and  $\phi_{il}$  are the magnitude and phase of the  $l$ th path of the channel leading to the  $i$ th antenna element, and  $\delta(t - \tau_{il})$  is a unit response for the propagation delay of  $\tau_{il}$ . The amplitude of the  $l$ th component can be Rayleigh (or Rician) distributed and the phase uniformly distributed between 0 and  $2\pi$ . The AWGN, generated at the  $i$ th antenna element is represented by  $v_i(t)$ .

As there are  $K_u$  simultaneous active users, the resultant received signal at the output of the  $i$ th antenna is the summation of the faded signals of all the users plus the Gaussian  $v_i(t)$  generated at the  $i$ th antenna

element:

$$r_i(t) = \sum_{k=1}^{K_u} (s_k(t) \otimes h_i^{(k)}(t)) + v_i(t) \quad (7)$$

For each antenna at the coherent receiver it is necessary to sample the received signals twice as fast as the transmitted samples one. Perfect frequency and timing receiver synchronisation are assumed. The receiver DFT operates on the  $2N$  samples as follows:

$$Z_{im} = \frac{1}{N} \sum_{u=0}^{2N-1} R_{iu} e^{-j(2\pi mu/2N)} \quad (8)$$

where  $R_{iu}$  is the  $u$ th sample of the received signal in the  $i$ th antenna,  $Z_{im} = y_{imp} - j y_{imq}$  and  $m = 0, 1, \dots, N-1$  represents the sub-carrier. Assuming a spreading code of length  $H$  for each antenna element, the resulting outputs are obtained by correlating the received signal of the  $m$ th sub-carrier against the spreading code of the desired user:

$$y_{im} = \sum_{h=0}^{H-1} [y_{imp}(h) c_{ph} - j y_{imq}(h) c_{qh}] \quad (9)$$

Despite the orthogonal property of the spreading code, the output of the correlator would not be zero because of the broken orthogonality induced by the channels. After the despreading, the signals of the different antennas input the space diversity combiner. The Viterbi algorithm [15] performs the maximal likelihood decoding of the values in the deinterleaver, which is fed by the combiner. Block interleaving was chosen in this simulation because in this the interleaver process randomises the channel and compensates for the fading effect.

### 2.3 Neural network space diversity combination

RNNs are dynamical systems with  $N_0$  external inputs and  $N_1$  fully interconnected neurons, as shown in Fig. 3. Artificial neural networks learn the statistical behaviour of the channel during a training period. The output of a neuron at time  $\hat{n} + 1$  depends on the external inputs to the network  $u_l(\hat{n})$ ,  $l = 1, 2, \dots, N_0$  and outputs of the neurons  $v_l(\hat{n})$ ,  $l = 1, 2, \dots, N_1$  at the previous time instant. The input vector  $u(\hat{n})$  and the output vector  $v(\hat{n})$  are concatenated to form  $g(\hat{n})$ :

$$g_l(\hat{n}) = \begin{cases} v_l(\hat{n}), & \forall l = 1, \dots, N_1 \\ u_{l-N_1}(\hat{n}), & \forall l = (N_1 + 1), \dots, (N_1 + N_0) \end{cases} \quad (10)$$

Two layers in the network may be distinguished, a concatenated input-output layer and a processing layer. There are a total of  $N_0 \times N_1$  forward connections and  $N_1^2$  feedback connections. Let  $w(\hat{n})$  denote the  $N_1 \times (N_0 + N_1)$  recurrent weight matrix of the network. The net internal activity of neuron  $k$  at time  $n$  is given by

$$\begin{aligned} net_k(\hat{n}) &= \sum_{l=1}^{N_1+N_0} w_{lk}(\hat{n}) g_l(\hat{n}) \\ &= \sum_{l=1}^{N_1} w_{lk}(\hat{n}) v_l(\hat{n}) + \sum_{l=1}^{N_0} w_{l+N_1,k}(\hat{n}) u_l(\hat{n}) \end{aligned} \quad (11)$$

where  $w_{lk}(\hat{n})$  is the estimate of the connection strength from the  $l$ th input to the  $k$ th neuron. At the next time step  $\hat{n} + 1$ , the output of neuron  $k$  at time  $\hat{n}$  is computed:

$$v_k(\hat{n} + 1) = f(net_k(\hat{n})) \quad (12)$$

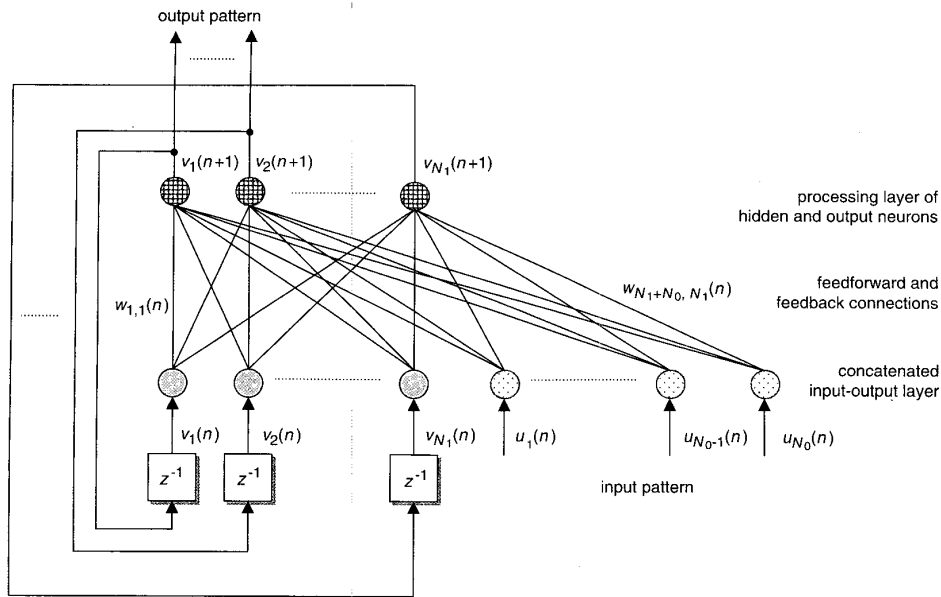


Fig. 3 Structure of real-time recurrent neural network

where the nonlinear activation function  $f(\cdot)$  is usually the sigmoid nonlinearity function:

$$f(net) = a \cdot \frac{1 - e^{-net \cdot b}}{1 + e^{-net \cdot b}} \quad (13)$$

Most algorithms proposed for RNNs use off-line training, where the weights are updated after a complete pass of the training data. In space diversity combining weights have to be updated in real time. The most widely known algorithm for online training of RNNs is the RTRL algorithm [10], and this is used here.

The optimum number of hidden neurons in the processing layer has been determined by heuristic methods, comparing the BER performance for different structures by Monte Carlo simulation. A system with three receiving antennas, and supporting eight synchronised users has been used. The channel conditions are determined by a Rician factor  $K=6$  dB. The RNN combiner is trained with a random sequence of 3200 symbols, at a SNR of 20 dB, obtaining the results after the training. The simplest of the RNN structures for a three-antenna-element receiver has two neurons in the processing layer and no neurons in the hidden layer. More complex structures, with hidden neurons, showed no improvement. The optimal value of the learning parameter  $\mu$  is also found by using heuristic techniques. For higher values of the learning rate, the convergence speed of the algorithm is faster and the achieved MSE is lower. However, the best BER performance is obtained for a learning rate  $\mu$  of 0.1.

The forgetting factor  $\alpha$  of the linear SRK algorithm [16, 17] has been set to 0.99. For smaller values of the  $\alpha$  parameter the performance of the diversity combiner becomes worse, because an error is rapidly propagated by means of the adaptation of the coefficients to an erroneous state. Owing to the back-propagation of the error, the system may become unstable in continuous transmission for  $\alpha$  values much lower than one. The length of the training data for the SRK combiner is assumed to be the same as the RNN system. The computational complexities of the RNN and the single-tap SRK structure are comparable, although

the SRK algorithm is simpler when a reduced number of antennas is used. The complexity of the RNN combiner increases linearly with the number of receiving antennas. The number of operations for the RNN combiner is mainly dependent on the number of output neurons, which is equal to two in all realisations. The complexity of CDMA neural networks is shown in the Appendix (Section 6.1).

### 3 Simulation results

The simulated multicarrier CDMA system uses sixteen sub-carriers, 16-QAM modulation, a carrier frequency of 900 MHz and a bit rate of 9.6 kbit/s. Each of the eight users spreads the information with its corresponding signature Walsh-Hadamard sequence of length 32. All simulations assume users with equal transmitting power. The value of the maximum Doppler frequency is 96 Hz.

Two ring TCM codes have been designed for simulation [9], the 64-state 012 200 232 030/132 and the 16-state 010 232 010/22 referred to as ring A and ring F, respectively, for simplicity. Two binary codes will be used for performance comparison, the 4-state 000 100 010/1001 and the 8-state 000 010 110 010/1100100, referred to as Ung G and Ung H. The decoder complexity is shown in the Appendix (Section 6.2).

This structure is applied to a multicarrier CDMA system with  $N$  receiving antennas. The RNN combining structure has  $N_0 = 2N$  external input connections because of the real and imaginary parts of the input vector. A hard-limiting decision device is located after the output of the network.

Fig. 4 shows the symbol error rate (SER) of different codes for a transmission over a channel of Rician factor  $K=10$  dB. The signals received in the three antenna elements are processed by the SRK algorithm. Codes A, F, G and H are applied at the transmitter and the receiver employs Viterbi decoding. The ring TCM code A outperforms the rest and also ring TCM F offers lower SER than the binary codes, both of which have a very similar SER. In all the cases, no improvement is achieved for SNRs higher than 10 dB. Fig. 5 shows the behaviour of coding in combination with the RNN diversity combiner. Ring TCM offers better results than binary codes.

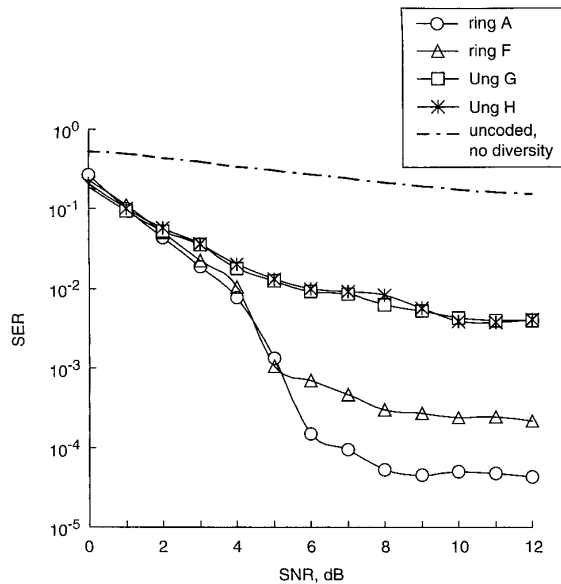


**Fig. 4** SER performance of Ungerboeck TCM and ring-TCM coded signals for eight users using three-antenna-element SRK combiner over non-frequency selective channel with  $K = 10$  dB

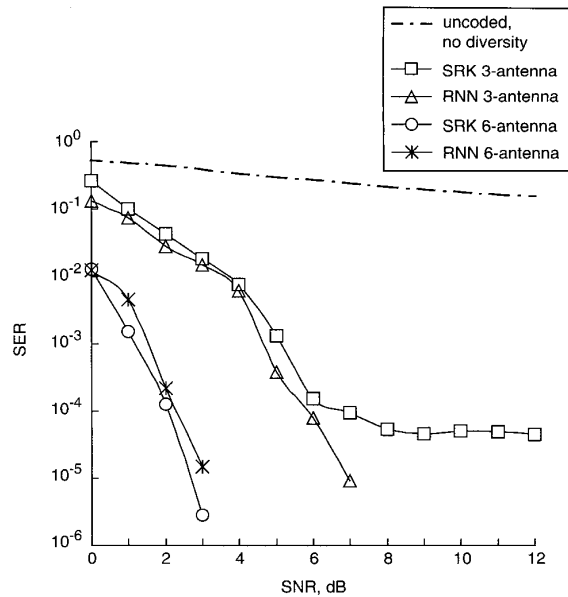


**Fig. 6** SER performance of ring-TCM A coded signals for eight users using three- and six-antenna-element SRK and RNN combiners over non-frequency selective channel with  $K = 10$  dB

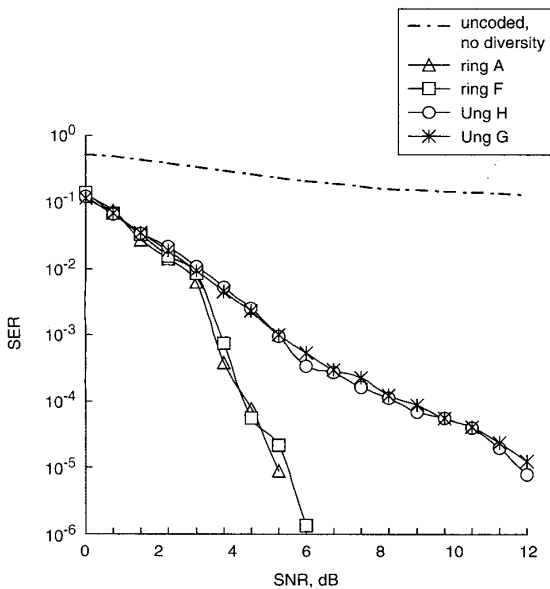


**Fig. 5** SER performance of Ungerboeck TCM and ring-TCM coded signals for eight users using three-antenna-element RNN combiner over non-frequency selective channel with  $K = 10$  dB

Fig. 6 compares the results of the two algorithms for ring code A only. For three antennas, the nonlinear method manages to continue improving the performance for SNRs higher than 10 dB, while the SRK reaches a flat region at that point. On the other hand, for a six-antenna element receiver, both algorithms give a similar outcome, though slightly better for the SRK algorithm.

Fig. 7 shows the SNR values needed to reach a SER of  $10^{-4}$ . For three antennas, only one of the integrated systems applying SRK algorithm achieves that point, and even in this case, it requires 1 dB more than the equivalent RNN

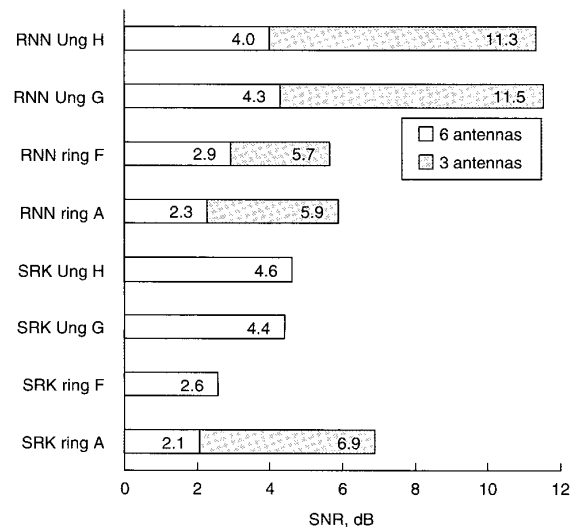


**Fig. 7** SNR required to reach SER of  $10^{-4}$  in multicarrier CDMA system over non-frequency selective channel with  $K = 10$  dB

system. For six-antenna systems the difference between the best codes is not remarkable, and both SRK and RNN need similar SNR. Anyhow, with regard only to the codes, there is a difference of around 2 dB in favour of ring TCM. This difference grows to more than 5 dB for three-antenna systems (taking into account only the RNN system, as the SRK algorithm is only able to offer such a SER with ring A encoding).

For ring TCM code F and the RNN diversity algorithm, Figs. 8 and 9 can be obtained. Coding on its own does not have too significant an influence on the receiver, but if coding is applied in conjunction with space diversity the advantage is considerable for both three and six antennas. In a more hostile environment, where the fading can be

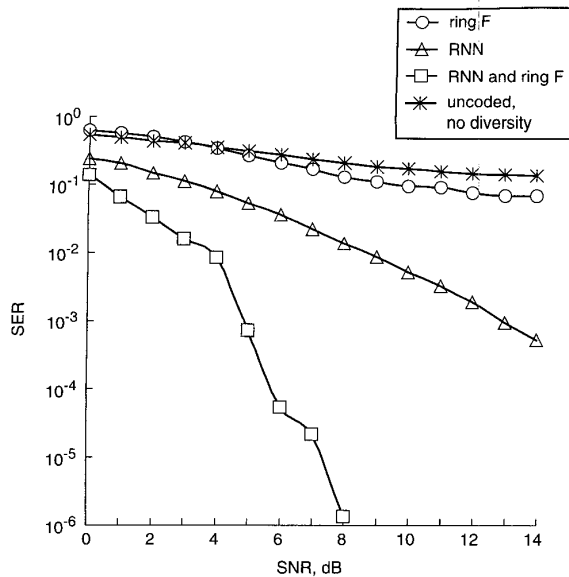


**Fig. 8** Influence of encoding process and space diversity working independently and in combination in multicarrier CDMA system with three-antenna-element combiner over non-frequency selective channel with  $K=10$  dB

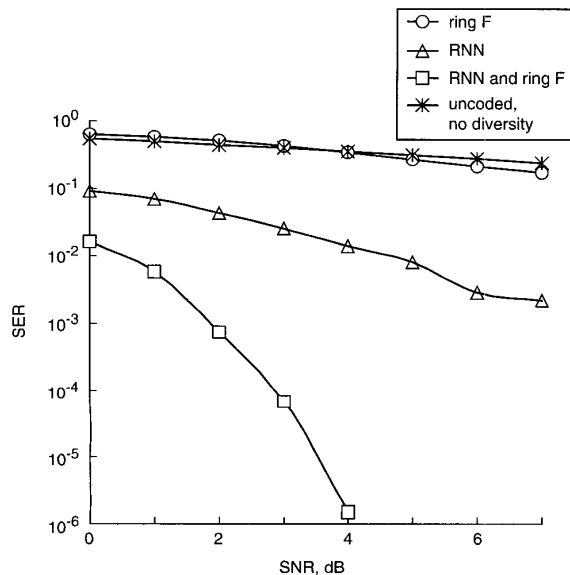


**Fig. 9** Influence of encoding process and space diversity working independently and in combination in multicarrier CDMA system with six-antenna-element combiner over non-frequency selective channel with  $K=10$  dB

considered as Rayleigh distributed, six-antenna devices also obtain a great benefit from the use of channel coding, as shown in Fig. 10.

There are two ways of performing space diversity combining: symbol rate combining and chip rate combining. For signal rate combining the symbols are combined after despreading, using matched filters in each of the diversity branches. In the case of chip rate combining, the adaptation of the diversity combining algorithm is performed for each chip, as suggested by Compton [13]. In this case, the diversity combiner is placed before the integration of the despread sequences. The chip rate

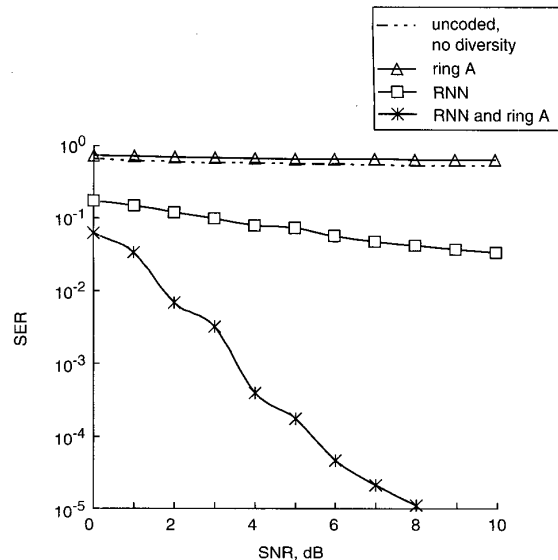


**Fig. 10** Influence of encoding process and six-element space diversity working independently and in combination in multicarrier CDMA system over non-frequency selective Rayleigh fading channel ( $K=0$  dB)

combiner requires a longer training sequence and requires more processing than the symbol rate combiner. Based on this, all of the subsequent investigations use diversity combiners operating at the symbol rate. For low values of the Rician factor, the SRK system becomes unstable due to the back-propagation of the error. Since it is not able to track the changes of the channel, it erroneously updates the coefficients of the algorithm because of both the lack of enough diversity and an inadequate value for the forgetting factor of the algorithm. A frequency selective fading channel with two fading paths, where the delay between them is equivalent to  $13.02 \mu\text{s}$ , has been assumed in Fig. 11.

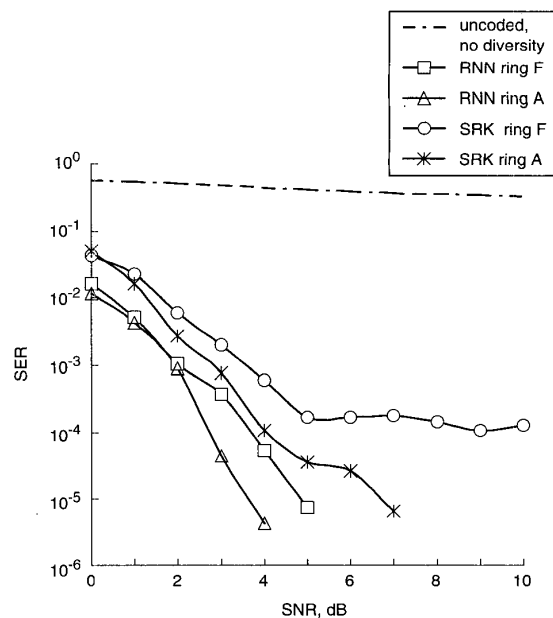


**Fig. 11** SER performance of ring-TCM coded signals for eight users using six-antenna-element SRK and RNN combiners over frequency selective channel with  $K=6$  dB

Each of these paths is at the same time, characterised by independent Rician fading of  $K = 6$  dB. The performance of the neural network is again superior to that of the SRK system.

#### 4 Conclusions

For the simulated multicarrier CDMA system transmitting over multipath fast fading channels, antenna diversity is used to remove the effects of multiple access interference, inter-symbol interference, and amplitude and phase distortion in the symbols. Ring TCM techniques implemented on top of the space diversity system are used to remove the possible remaining errors.

Results show that when providing enough space diversity for channels with a high Rician factor, both combining algorithms perform similarly. Smaller values of  $K$  make the SRK system unstable and RNN is the only valid option. For three-antenna-element receiver arrays, superior performance of the RNN over the fading channels system becomes clearer. For high Rician factors, the linear system no longer offers any considerable performance improvement over the RNN algorithm. For example, over non-frequency selective channels with  $K = 10$  dB, the SRK reaches its best performance by a SNR equal to 10 dB, while the RNN continues improving until 16 dB. In addition to this, and continuing with this example, the SRK combined with binary coding never achieves a SER lower than  $2 \times 10^{-3}$ , while the RNN reaches  $10^{-4}$  with a SNR of 12 dB and an SER performance of  $10^{-5}$  with a SNR of 16 dB.

The superior performance offered by the RNN structure in channels dominated by multipath fading, inter-symbol interference and multiple access interference can be explained by its ability to form complex nonlinear decisions.

Finally, when one comes to the subject of the optimum encoding interleaving techniques, the coded space diversity systems using ring TCM and binary TCM encoding have been evaluated, proving to be a good coding scheme for fading channels. In order to achieve the best possible performance, it is important to choose an encoding scheme that adequately suits the RNN diversity combiner.

#### 5 References

- BINGHAM, J.A.: 'Multicarrier modulation for data transmission: an idea whose time has come', *IEEE Commun. Mag.*, May 1990
- WIDROW, B., MANTEY, P.E., GRIFFITHS, L.J., and GOODE, B.B.: 'Adaptive antenna systems', *Proc. IEEE*, December 1967, **55**, (12), pp. 2143-2159
- THOMPSON, J.S., GRANT, P.M., and MULGREW, B.: 'Performance of antenna array receiver algorithms for CDMA', *Signal Process.*, 1998, **68**, pp. 23-41
- WIDROW, B., and HOFF, M.E. Jr.: 'Adaptive switching circuits'. Proceedings of Institute of Radio Engineers, Western Electronic Show and Convention, IRE WESCON, August 1993, pp. 96-104
- MUELLER, M.S.: 'Least-squares algorithms for adaptive equalizers', *Bell Syst. Tech. J.*, October 1981, **60**, pp. 1905-1925
- BENSON, M., and CARRASCO, R.A.: 'Application of recurrent neural networks to space diversity in SSDMA and CDMA mobile communication systems', *Neural Comput. Appl.*, 2001, **10**, pp. 136-147
- BALDINI, R.F., and FARRELL, P.G.: 'Coded modulation with convolutional codes over rings'. Presented at Second IEE Bangor Symposium on Communications, Bangor, Wales, May 1990
- MASSEY, J.L., and MITTELHOLZER, T.: 'Codes over rings: a practical necessity'. Presented at AAECC7 International Conference, Toulouse, France, Université P. Sabatier, June 1989
- SOTO, I., and CARRASCO, R.A.: 'Searching for TCM codes using genetic algorithms', *IEE Proc., Commun.*, February 1997, **144**, (1), pp. 6-10
- CARRASCO, R.A., and SOTO, I.: 'Design of TCM codes and interleaving processes for fading channels using genetic algorithms', *Int. J. Commun. Syst.*, 1998, **11**, pp. 311-318

- WILLIAMS, R.J., and ZIPSER, D.: 'A learning algorithm for continually running fully recurrent neural networks', *Neural Comput.*, 1989, **1**, pp. 270-280
- FORNEY, G.D. Jr., and WEI, L.F.: 'Multidimensional constellations - Part I: Introduction, figures of merit, and generalized cross constellations', *IEEE J. Sel. Areas Commun.*, August 1989, **7**, (6), pp. 877-892
- COMPTON, R.T.: 'Adaptive antennas, concepts and performance' (Prentice Hall, 1988)
- HARA, S., and PRASAD, R.: *IEEE Commun. Mag.*, 1997, **35**, (12), pp. 126-133
- VITERBI, A.J.: 'Error bound for convolutional codes and asymptotically optimum decoding algorithm', *IEEE Trans. Inf. Theory*, 1967, **13**, (2), pp. 260-269
- HSU, F.M.: 'Square root Kalman filtering for high-speed data received over fading dispersive HF channels', *IEEE Trans. Inf. Theory*, September 1982, **28**, (5)
- HAYAN, M.T., DEMUTH, H.B., and BEALE, M.: 'Neural network design' (PWS Publishing Company, 1996)
- FELTWEIS, G., and MEYR, H.: 'Parallel Viterbi algorithm implementation: breaking the ACS bottleneck', *IEEE Trans. Commun.*, August 1989, **37**, (8), pp. 785-789

#### 6 Appendix

##### 6.1 Complexity of CDMA neural networks

Table 1 shows the total number of mathematical operations per input pattern required to implement the SRK/RTRL algorithms. The operations required for the combining algorithms investigated are presented in Table 2 for different numbers of receiving antenna elements. The RNN structure has no hidden neurons. Note that the computational complexities are obtained assuming that the evaluation of a sigmoid function requires the equivalent of ten floating point operations. The computational complexities of the RNN and the single-tap SRK structure are comparable.

**Table 1: Mathematical operations for implementing algorithms**

Algorithm	Multiplications	Additions	Sigmoid functions
SRK	$6N_c^2 + 12N_c$	$6N_c^2 + 4N_c$	—
RTRL	$(N_1 + N_0)(N_1 + 2N_1^2 + 2N_1^2)$	$(N_1 + N_0)(N_1 + N_1^2 + N_1^2)$	$N_1$

$N_c$  is the total number of diversity combiner's coefficients,  $N_0$  is the number of external inputs and  $N_1$  is the number of output neurons.

**Table 2: Algorithm operations required for different numbers of receiving antenna elements**

No. of antennas	2	3	4	5	6	7	8
SRK	80	156	256	380	528	700	896
RTRL	260	340	420	500	580	660	740

##### 6.2 Ring-TCM and conventional 2-D TCM Viterbi decoder complexity

Two main aspects must be analysed in order to determine the complexity of the Viterbi decoding process [18] of conventional 2-D TCM codes and ring-TCM codes as shown in Table 3: the computational requirements, i.e. the number of arithmetic operations needed to carry out the

**Table 3: Decoder complexity**

<i>nst</i>	<i>c</i> (conv)	<i>c</i> (ring)	<i>npar</i> (conv)	<i>CPBM</i> (conv)	<i>CACS</i> (conv)	<i>npar</i> (ring)	<i>CPBM</i> (ring)	<i>CACS</i> (ring)
4	4.0	4.7	4	8	12	16	12	14
8	6.0	6.64	4	8	56	8	40	60
16	6.91	7.32	2	8	112	8	40	120
64	8.83	10.01	2	8	448	4	40	992

*npar* values are the parallel transitions of the trellis, *CPBM* is the normalised complexity of the PBM, *CACS* values are the normalised computational intensities of conventional 2-D TCM codes and ring-TCM codes suitable for multi-level QAM, *c*(conv) values are the normalised complexities of conventional 2-D TCM, and *c*(ring) values are the ring-TCM VDs, which are slightly superior to those of the conventional TCM, and *nst* is the number of states of the trellis.

research for the shortest path in the trellis, and also the memory requirements, i.e. the number of storage locations needed to keep track of the surviving paths and to save the current state metrics. In order to analyse the computational burden of a Viterbi decoder (VD), it is convenient to break its basic structure into three functional units:

- (i) Computational unit of the parallel branch metric (PBM);
- (ii) Add-compare-select (ACS) unit;
- (iii) Decoder frame output (DFO) unit.

Table 3 shows the decoder complexity.